Optimizing the Synthesis of Red- to Near-IR-Emitting CdS-Capped $CdTe_xSe_{1-x}$ Alloyed Quantum Dots for Biomedical Imaging

Wen Jiang,[†,||] Anupam Singhal,[‡,||] Jianing Zheng,[§] Chen Wang,[§] and Warren C. W. Chan*[,†,⊥]

Institute of Biomaterials & Biomedical Engineering, Department of Materials Science and Engineering, University of Toronto, Toronto, Ontario, Canada, Department of Pathology and Laboratory Medicine, Mount Sinai Hospital, Toronto, Ontario, Canada, and Department of Chemical Engineering, University of British Columbia, British Columbia, Canada

Received June 5, 2006. Revised Manuscript Received August 1, 2006

Advancements in biomedical imaging require the development of optical contrast agents at an emission region of low biological tissue absorbance, fluorescence, and scattering. This region occurs in the red to near-IR (>600 nm) wavelength window. Quantum dots (Qdots) are excellent candidates for such applications. However, there are major challenges with developing high optical quality far-red- to near-IR-emitting Qdots (i.e., poor reproducibility, low quantum yield, and lack of photostability). Our aim is to systematically study how to prepare alloyed $CdTe_xSe_{1-x}$ with these properties. We discovered that the precursor concentrations of Te-to-Se and growth time had major impacts on the Qdot's optical properties. We also learned that the capping of these alloyed Qdots were difficult with ZnS but feasible with CdS because of the ZnS's lattice mismatch with the $CdTe_xSe_{1-x}$. These systematic and basic studies led to the optimization of synthetic parameters for preparing Qdots with high quantum yield (>30%), narrow fluorescence full width at half-maxima (<50%), and stability against photobleaching (>10 min under 100W Hg lamp excitation with a 1.4 numerical aperture 60× objective) for biomedical imaging and detection. We further demonstrate the conjugation of biorecognition molecules onto the surface of these alloyed Qdots and characterize their use as contrast agents in multicolored and ultrasensitive imaging.

Introduction

The red to near-infrared (IR) wavelength window (600−900 nm) is rapidly emerging as an important region of the electromagnetic spectrum for biological imaging and detection. Optical imaging using visible light is hampered by native biological fluorescence ("autofluorescence") as well as light absorption and scattering by biological tissue constituents, such as amino acids, blood hemoglobin, and water; however, near-IR-emitting fluorescence imaging overcomes these challenges, because biological autofluorescence and absorbance are both at their minima in the wavelength range of 600−900 nm. This region of the spectrum is referred to as the red- to near-infrared-emitting "window".[1−5] Traditional imaging applications using near-IR light were primarily achieved with organic fluorescence probes. Organic fluorophores such as the Cyanine and Alexa dye series have provided important contributions to near-IR-emitting optical imaging.[6−8] Ultrasensitive and deep penetration cell and tissue imaging have already been demonstrated using these fluorophores.[9,10] Unlike visible-emitting organic fluorophores, there are relatively few near-IR-emitting organic fluorophores available. Furthermore, these near-IR-emitting organic fluorophores tend to photobleach and have a narrow absorption profile and broad emission full width at half-maximum (fwhm).[8] These problems limit the use of current organic-based near-IR-emitting fluorophores for ultrasensitive and multiplexed biological imaging in cells, tissues, and whole animal.

With the introduction of quantum dots (Qdots) to the biological community, the ability to design near-IR-emitting fluorescence probes was expected to be rather simple, because the optical emission of Qdots can be tuned by size, shape, and composition. The ZnS-capped CdSe Qdots series has excellent optical qualities (i.e., narrow emission spectra, photostable, and broad absorption spectra) for biological imaging and detection;[11−16] however, at the current state, we and others have found that the far-red- to near-Ir-

* To whom correspondence should be addressed. E-mail: warren.chan@utoronto.ca.
† Institute of Biomaterials & Biomedical Engineering, University of Toronto.
|| These two authors contributed equally to this work.
‡ University of British Columbia.
§ Mount Sinai Hospital.
⊥ Department of Materials Science and Engineering, University of Toronto.

(1) Frangioni, J. V. *Curr. Opin. Chem. Biol.* **2003**, *7*, 626−634.
(2) Chance, B. *Ann. N. Y. Acad. Sci.* **1998**, *838*, 29−45.
(3) Weissleder, R. *Nat. Biotechnol.* **2001**, *19*, 316−317.
(4) Weissleder, R.; Ntziachristos, V. *Nat. Med.* **2003**, *9*, 123−128.
(5) Jiang, W.; Papa, E.; Fischer, H.; Mardyani, S.; Chan, W. C. W. *Trends Biotechnol.* **2004**, *23*, 607−609.
(6) Zaheer, A.; Wheat, E. T.; Frangioni, J. V. *Mol. Imaging* **2002**, *1*, 354−364.
(7) Nakayama, A.; Bianco, A. C.; Zhang, C.; Lowell, B. B.; Frangioni. J. V. *Mol. Imaging* **2003**, *2*, 37−49.
(8) Mujumdar, B. R.; Ernst, L. A.; Mujumdar, R. S.; Lewis, J. C.; Waggoner, S. A. *Bioconj. Chem.* **1993**, *4*, 105−111.
(9) Zaheer, A.; Lenkinski, R. E.; Mahmood, A.; Jones, A. G.; Cantley, L. C.; Frangioni, J. V. *Nat. Biotechnol.* **2001**, *19*, 1148.
(10) Hilger, I.; Leistner, Y.; Berndt, A.; Fritsche, C.; Haas, K. M.; Kosmehl, H.; Kaiser, W. A. *Eur. Radiol.* **2004**, *14*, 1124.
(11) Chan, W. C. W.; Nie, S. *Science* **1998**, *281*, 2016−2018.
(12) Chan, W. C. W.; Maxwell, D. J.; Gao, X.; Bailey, R. E.; Han, M.; Nie, S. *Curr. Opin. Biotechnol.* **2002**, *13*, 40−46.
(13) Bruchez, J. M.; Moronne, M.; Gin, P.; Weiss, S.; Alivisatos, A. P. *Science* **1998**, *281*, 2013−2016.
(14) Gao, X.; Cui, Y.; Levenson, R. M.; Chung, L. W. K.; Nie, S. *Nat. Biotechnol.* **2004**, *22*, 969−976.
(15) Akerman, M. E.; Chan, W. C. W.; Laakkonen, P.; Bhatia, S. N.; Ruoslahti, E. *Proc. Natl. Acad. Sci., U.S.A.* **2002**, *99*, 12617−12621.

10.1021/cm061311x CCC: $33.50
Published on Web 09/08/2006

emitting Qdots are technically challenging to synthesize and do not have the same advantageous optical properties for biological imaging and detection. For example, both Ellisman and co-workers and Gambhir and co-workers measured the fluorescence emission of commercial near-IR-emitting Qdots.[17−19] They showed that the 700 nm emitting biocompatible Qdots have a fluorescence full width at half-maximum 4 times greater than that of the visible emitting Qdots. Similarly, Kim et al. showed similar broad emission spectra for their biocompatible near-IR-emitting Qdots.[20−22] Also, Geho et al. showed that the 655 nm red-emitting Qdots are not stable in aqueous solvents and shift in fluorescence to blue.[23] CdTe Qdots, although they can be synthesized to have emission wavelength ranging from 580 to 770 nm under the right experimental conditions,[24] are prone to degradation. Te can be easily oxidized under ambient conditions.[25] Recently, Bailey et al. reported the synthesis of near-IR-emitting alloyed CdTeSe Qdots that overcomes these problems.[26,27] However, the water-solubilization of these Qdots led to a dramatic loss of fluorescence, and the long-term stability of these Qdots are in question because of the lack of capping layer. For biological applications, the far-red- to near-IR-emitting Qdots must have specific optical properties if they are to be useful in biological and biomedical research. The Qdots must have high quantum yield (>30% in aqueous solvents) and narrow emission (<50 nm) and be photostable (does not lose fluorescence) and nontoxic (which means that the alloyed Qdots have to be capped with a low photo-oxidation shell).[28] Thus far, to the best of our knowledge, there are no quantitative data within the literature that demonstrate all of these properties for a series of red- to near-IR-emitting Qdots. Because of the need for a highly luminescent and stable optical probe in this biomedically and biologically important region, we set out to study the kinetics of red- to near-IR-emitting Qdot synthesis and growth to obtain information on preparing red- to near-IR-emitting Qdots with the specified optical properties. Of all these properties, we discovered that the narrow emission wavelengths are the most difficult to obtain. For this alloyed system, sub-50 nm is achieved when the temperature is quickly decreased right after the injection of precursors (<1−2 min).

Experimental Section

Materials. Selenium powder (Se, 99.5%), hexamethyldisilathiane, trioctylphoshpine (TOP, tech. 90%), tri-*n*-octylphosphine oxide (TOPO, tech. 90%), tellurium powder (99.8%), mercaptoundecanoic acid (MUA, 95%), DL-lysine (98%), 1,3-dicyclohexylcarbodiimide (DCC) (99%), human apo-transferrin (≥97%), *N*-(3-dimethylaminopropyl)-*N*-ethylcarbodiimide hydrochloride (EDC, commercial grade), Sephadex G-75 columns, phosphate buffered saline (PBS), Dulbecco's minimum essential media (DMEM), fetal bovine serum (FBS), amphotericin B, penicillin−streptomycin, 0.25% trypsin−EDTA solution, and IR-786 perchlorate were purchased from Sigma-Aldrich (St. Louis, MO). Dimethylcadmium (DMC, min. 97%) was purchased from Strem Chemicals (Newburyport, MA). Chloroform, methanol, acetone (ACS grade), and paraformaldehyde were purchased from EMD Chemicals Inc. (Gibbstown, NJ). Cy5.5 mono-NHS ester was purchased from Amersham Biosciences (Buckinghamshire, U.K.). ICP standard solutions of Cd, Se, and Te were from High-Purity Standard (Charleston, SC).

Synthesis of $CdTe_xSe_{1-x}$/CdS Qdots. Unless otherwise specified, all reactions were done in an inert argon atmosphere. TOPO (20 g) was placed into a 125 mL glass three-necked flask and heated to 150 °C, after which 0.888 mmol of DMC was injected into the flask. After the mixture was stirred for 15 min, the temperature was raised to 325 °C. The ratio of total cadmium to selenium and tellurium in the mixture was kept constant at 6:1. Five different Se and Te mixtures were prepared with molar ratios of 0:100, 33:66, 50:50, 66:33, and 75:25. The injection of these different mixtures of Se and Te precursor solutions into the reaction vessel resulted in immediate nucleation of Qdots with an emission range of 580 to 750 nm. To cap these Qdots with an inorganic shell, the reaction temperature was lowered to 280 °C, at which 500 μL of TOP ($TMS_2(S)$) was injected dropwise into the reaction vessel. The lowering of the reaction temperature and dropwise injection of TOP-($TMS_2(S)$) were to reduce the degree of homogeneous nucleation of CdS crystals. The final solution was left in the reaction vessel at 100 °C for 1−2 h, and size selective washing was performed using methanol (typically methanol washing can reduce the fwhm of the final Qdots sample by 10−15%).

Surface Modification of Qdots. The surface of the $CdTe_xSe_{1-x}$/CdS Qdots was modified to render them water soluble and biocompatible using previously developed techniques.[29] Briefly, TOPO-coated $CdTe_xSe_{1-x}$/Cds Qdots were dissolved in chloroform and mixed with MUA at a molar ratio of ∼1:20 000. The MUA displaced the TOPO molecules on the Qdot surface and rendered them soluble in an intermediate polar solvent such as dimethyl sulfoxide (DMSO). The Qdot solution was then mixed with lysine (16 000 molar excess to Qdots) and DCC (5 molar excess of lysine) for 2 h. This led to the cross-linking of the carboxylic acid terminating ends of the MUA on the Qdot surface, creating an organic "shell" around the Qdots. The resulting lysine cross-linked MUA Qdots were soluble in aqueous solvent. For detailed protocol and characterizations, see ref 29.

Conjugation with the Protein Transferrin and Cell Studies. Six-hundred-seventy nanometer emitting and 750 nm emitting Qdots were separately conjugated to transferrin using EDC. Briefly, 15 μL of Qdot solutions was mixed with transferrin (10 mg/mL) in a

(16) Voura, E. B.; Jaiswal, J. K.; Mattoussi, H.; Simon, S. M. *Nat. Med.* **2004**, *10*, 993−998.
(17) Giepmans, B. N.; Deerinck, J. T.; Smarr, L. T.; Jones, Z. Y.; Ellisman, H. M. *Nat. Methods* **2005**, *2*, 743−749.
(18) So, M.; Xu, C.; Loening, A. M.; Gambhir, S. S.; Rao, J. *Nat. Biotechnol.* **2006**, *24*, 339−343.
(19) Cai, W.; Shin, D. W.; Chen, K.; Gheysens, O.; Cao, Q.; Wang, S. X.; Gambhir, S. S.; Chen, X. *Nano Lett.* **2006**, *6*, 669−676.
(20) Kim, S.; Fisher, B.; Eisler, H. .J.; Bawendi, M. G. *J. Am. Chem. Soc.* **2003**, *125*, 11466−11467.
(21) Kim, S.; Lim, Y. T.; Soltesz, E. G.; De Grand, A. M.; Lee, J.; Nakayama, A.; Parker, A. J.; Mihajevic, T.; Laurence, R. G.; Dor, D. M.; Cohn, L. H.; Bawendi, M. G.; Frangioni, J. V. *Nat. Biotechnol.* **2004**, *22*, 93−97.
(22) Lim, Y. T.; Kim, S.; Nakayama, A.; Stott, N. E.; Bawendi, M. G.; Frangioni, J. V. *Mol. Imaging* **2003**, *2*, 50−64.
(23) Geho, D.; Lahar, N.; Gurnani, P.; Huebschman, M.; Herrmann, P.; Espina, V.; Shi, A.; Wulfkuhle, J.; Garner, H.; Petricoin, E.; Liotta, L. A.; Rosenblatt, K. P. *Bioconjugate Chem.* **2005**, *16*, 559.
(24) Mikulec, F. V.; Bawendi, M. G.; Kim, S. Patent WO 01/07689 A2.
(25) Rogach, A. L.; Talapin, D. V.; Weller, H. *Colloids and Colloid Assembly;* Caruso, F., Ed.; Wiley-VCH: Weinheim, Germany, 2004.
(26) Bailey, R. E.; Strausburg, J. B.; Nie, S. *J. Nanosci. Nanotechnol.* **2004**, *4*, 569−574.
(27) Bailey, R. E.; Nie, S. *J. Am. Chem. Soc.* **2003**, *125*, 7100−7106.
(28) Derfus, A. M.; Chan, W. C. W.; Bhatia, S. N. *Nano Lett.* **2004**, *4*, 11−18.
(29) Jiang, W.; Mardyani, S.; Fischer, H.; Chan, W. C. W. *Chem. Mater.* **2006**, *18*, 872−878.

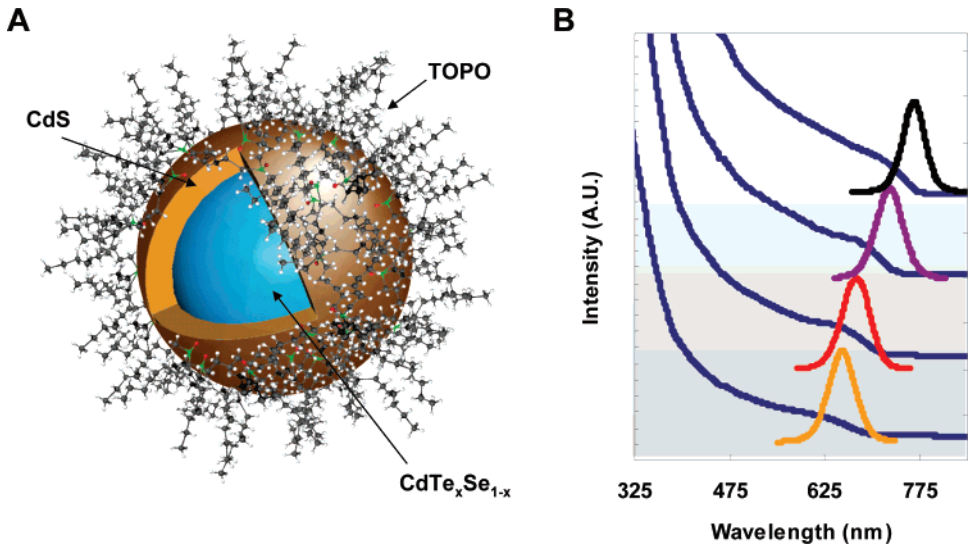

Figure 1. Schematic and optical properties of CdS-capped $CdTe_xSe_{1-x}$ alloyed near-IR-emitting Qdots. (A) Biocompatible near-IR-emitting Qdots contain a core structure ($CdTe_xSe_{1-x}$) with a CdS and an organic shell. The outer organic shell contains functional groups for attaching biorecognition molecules to the Qdot surface. (B) Absorbance and fluorescence spectra of CdS-capped $CdTe_xSe_{1-x}$ near-IR-emitting Qdots with different compositions of Te:Se in the core.

molar ratio of 1:25. EDC was then mixed with the Qdot−transferrin solution at a 10 times molar excess of protein. The mixtures were stirred for 2 h and filtered using Sephadex G-75 gel filtration columns. The Qdot−transferrin bioconjugates were then incubated with HeLa cells (30−50% confluent cultured in 15 mm × 100 mm tissue culture dish) overnight in 5% CO_2 at 37 °C, and HeLa cells were cultured in Dulbecco minimum essential media (DMEM) with 10% fetal bovine serum, 1% penicillin, and 1% amphotericin B. Unconjugated Qdots and Qdots conjugated to bovine serum albumin (BSA) were incubated with HeLa cells and served as controls. After the incubation was completed, the stained HeLa cells were trypsinized and washed with PBS (10 mM, pH 7.4). The cells were fixed using 4% paraformaldehyde and then spread on a cover glass and imaged using epifluorescence microscope.

Characterizations. Optical absorption spectra of the far-red- to near-IR-emitting Qdots were measured using the Shimadzu UV-1601PC UV−visible spectrophotometer (Shimadzu, Japan). Fluorescence measurements were obtained with the Fluoromax-3 spectrofluorimeter (Jobin Yvon, Horiba). Fluorescence images were obtained using the Olympus IX71 inverted microscope with a 1.4 numerical aperture 60× objective, 100 W Hg lamp, and Coolsnap CCD camera. ICP-AES analysis was performed using Optima 3000 ICP AES system. Hitachi HD2000 STEM was used to obtain the transmission electron microscopy images of the Qdots. All Qdot samples were spread on carbon-coated copper grids. EDX data were gathered using a Hitachi HD2000 STEM equipped with Inca EDX system. PXRD analysis was performed using an automated Siemens/Bruker AXS D5000 diffractometer. The Qdot samples were dried and then deposited on a low-background sample holder. All samples were run in a step scan mode, with a scan range (2) of 15−75° and step size of 0.02°.

Results and Discussion

Synthesis of Far-Red- to Near-IR-Emitting Core Alloyed $CdTe_xSe_{1-x}$ Qdots. High-quality near-IR-emitting $CdTe_xSe_{1-x}$ Qdots were synthesized by injecting a mixture of dissolved selenium and tellurium into a hot coordinating solvent of trioctylphosphine oxide (TOPO) containing dimethylcadmium. The Qdots consist of an alloyed $CdTe_xSe_{1-x}$ core with a CdS shell and have emission wavelengths that can be tuned from 600 to 850 nm (Figure 1). To prepare these alloyed Qdots with the desired emission wavelengths and optical properties, we studied the growth kinetics of the alloyed Qdots. In the reaction vessel, the formation of the Qdots was readily apparent by the change in the color of the reaction mixture from clear to dark red and the shift of the emission toward longer wavelength (Figure 2). For binary visible emitting Qdots, multiple injections of precursor solutions are commonly used to increase the size of the Qdots and to shift their fluorescence emission to red. However, with alloyed Qdots, multiple injections of monomers into the reaction vessel during growth caused a rapid reduction in the homogeneity of the nanocrystals and broadening of the fluorescence full width at half-maxima (fwhm) (see Figure 3). Unlike the binary CdSe Qdots, the growth kinetics of the alloyed $CdTe_xSe_{1-x}$ is dependent upon three chemical reactants (Cd, Te, and Se) and their relative concentrations in the reaction vessel. These variables may contribute to the poor optical qualities of most of the reported far-red- to near-IR-emitting alloyed Qdots.

During Qdots synthesis, we monitored the change in the relative concentration of Te:Se in the alloyed Qdots after precursor injection. Using inductively coupled plasma atomic emission spectrometry (ICP-AES), we determined the concentration of Te and Se in the alloyed Qdots and compared it to the initial precursor concentrations. Regardless of the Te:Se injection ratio, we always observed the predominance of Te within the alloyed core structure immediately upon Qdot nucleation (Figure 4). The initial composition of the alloyed Qdots consisted of 73% Te when the concentration of Te was twice the concentration of Se in the injected precursor solution. Similarly, equimolar precursor concentrations of the Te and Se produced alloyed Qdots with 65% Te after nucleation; precursor solutions containing a concentration of Se twice that of Te produced alloyed Qdots with 59% Te after nucleation. These results suggest that Te reacts much faster with Cd relative to Se. Figure 4 also indicates that the equilibrium between the Te:Se concentrations in the alloyed

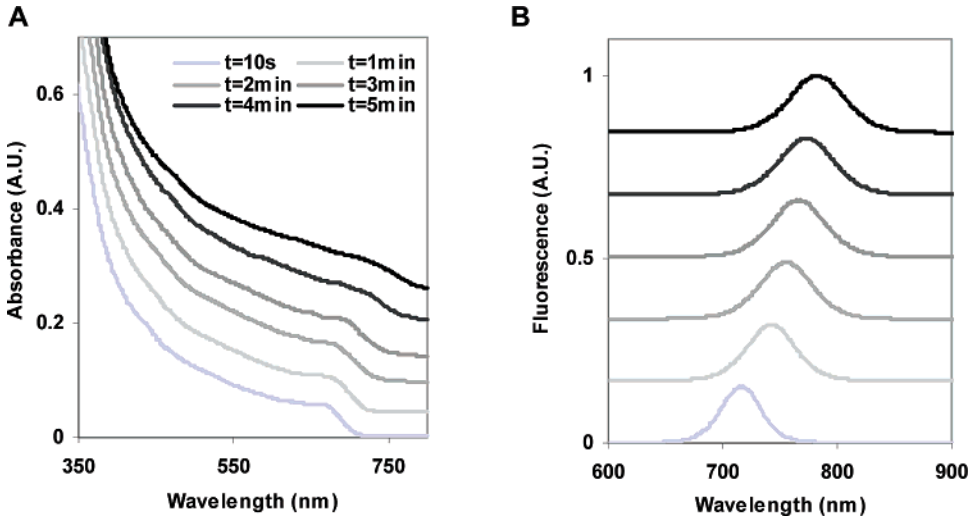

Figure 2. Evolution of the optical properties of the near-IR-emitting Qdots with respect to reaction time. (A) Change in the absorption profile of the Qdots with respect to reaction time. (B) Change in the emission profile of the Qdots with respect to reaction time.

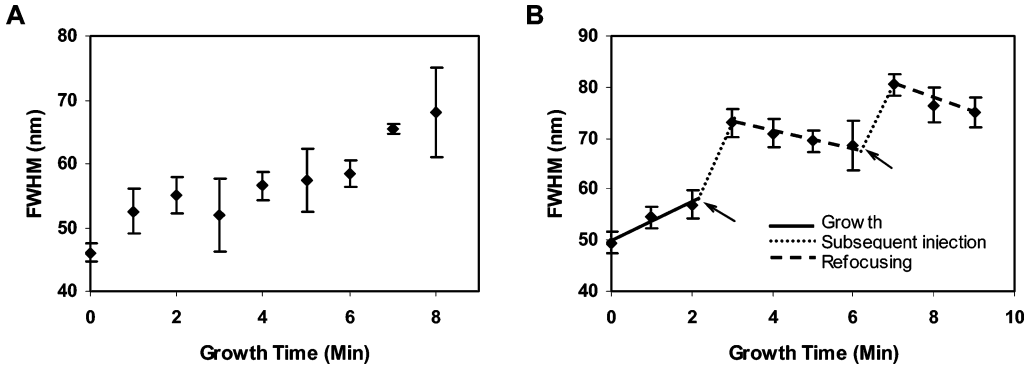

Figure 3. Impact of growth time and precursor injection frequencies on the fluorescence fwhm of the alloyed near-IR-emitting Qdots. (A) Fluorescence fwhm of the near-IR-emitting Qdots broadens for extended Qdot growth times. (B) Repeated injections (indicated by the arrows) of precursor solutions into the reaction vessel caused sharp increases in the width of the Qdot's fluorescence fwhm. This significant increase in the fluorescence-emission fwhm was followed by a "refocusing" phase, where the fluorescence fwhm narrowed. Further narrowing of the fwhm of the alloyed near-IR-emitting Qdots can be achieved by size-selective precipitation.

Qdots is reached after longer growth times. After equilibrium is reached, we observed the final composition of the alloyed Qdots to follow that of the initial precursor-injection concentrations. As expected, the change in Te and Se composition during growth was reflected in the emission wavelength of the Qdots. In Figure 5, we showed that the emission wavelengths of the Qdots have a strong correlation with the composition of Te and Se of the nanocrystal. Higher Se composition in the precursors led to the formation of longer wavelength Qdots (Figure 5).

Because the Se to Te ratio in the precursor solution had a strong effect on the wavelength of the Qdots immediately after nucleation, the tuning of the optical emission of the Qdots by precursor concentrations was feasible. Apart from composition tuning of the emission wavelengths, which has been confirmed by Bailey and Nie,[27] we demonstrated that the emission of the alloyed $CdTe_xSe_{1-x}$ Qdots can also be tuned by altering the Qdot size as is typically done with binary Qdots (e.g., CdSe). Size-based tuning of the fluorescence emission was confirmed using TEM in conjunction with fluorimetry to examine aliquots of $CdTe_xSe_{1-x}$ Qdots at different growth times postnucleation. Figure 6 shows the growth profile for different composition of $CdTe_xSe_{1-x}$ Qdots immediately after nucleation (within 10 s after the initial precursor injection) and their corresponding wavelengths. The rate of the nanocrystal growth is also dependent on the Qdot composition, possibly because of the difference in reactivity between Te and Se. These results indicate that the fluorescence emission of alloyed $CdTe_xSe_{1-x}$ Qdots can be tuned by size, composition, or a combination of both, by carefully selecting the right amount and ratio of precursors and growth time. On the basis of these studies, we conclude that the fluorescence emission of these alloyed Qdots can be tuned by (1) changing the Te:Se molar ratio in the precursor mixtures and/or (2) changing the growth time.

Powdered X-ray diffraction (PXRD) was further used to confirm the structure and compositions of the alloyed Qdots (see Figure 7). These PXRD data indicate that $CdTe_xSe_{1-x}$ alloyed Qdots have a wurtzite structure similar to that of binary CdSe and CdTe Qdots. This is in agreement with previous reports.[27] A shift in the PXRD spectra toward the CdTe or CdSe Qdots is observed when the Te or Se concentration, respectively, dominates. As in the case of $CdTe_{0.3}Se_{0.7}$ Qdots, the diffraction peaks shifted approximately 2θ from pure CdSe peaks toward the pure CdTe peaks (Figure 7). These alloyed Qdots are monodisperse (see

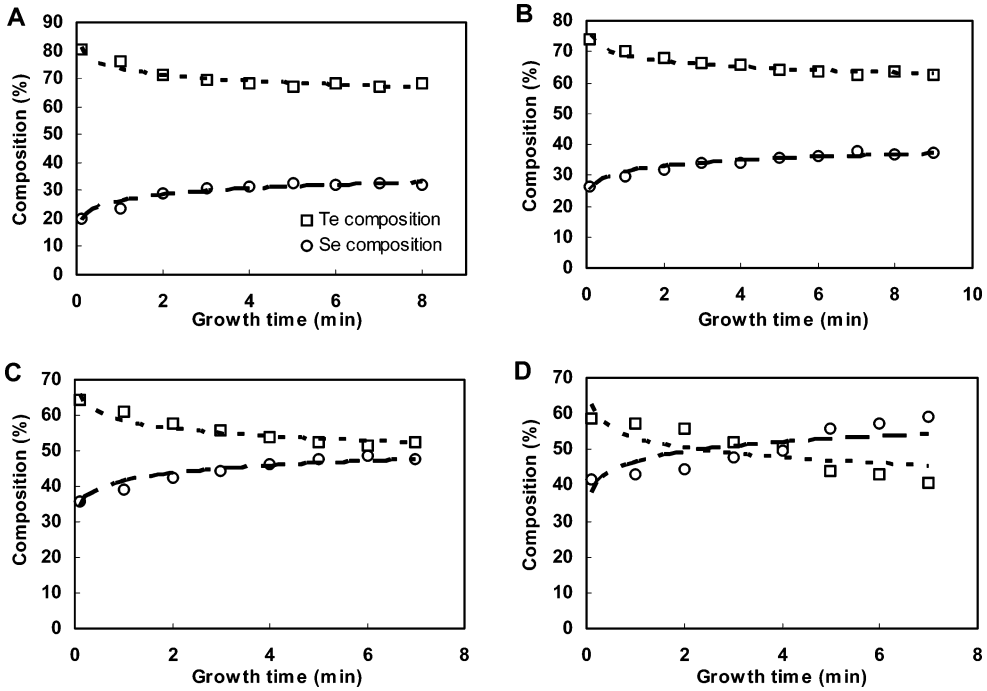

Figure 4. ICP-AES analysis of the Te:Se ratio of the near-IR-emitting Qdots at nucleation and during subsequent growth. (A−D) Qdots with different initial precursor injection compositions, corresponding to $CdTe_{0.66}Se_{0.33}$, $CdTe_{0.6}Se_{0.4}$, $CdTe_{0.5}Se_{0.5}$, and $CdTe_{0.33}Se_{0.66}$, respectively. Regardless of the injection Te:Se ratio in the injected precursor concentrations, Te dominates the composition of the $CdTe_xSe_{1-x}$ upon nucleation. However, equilibrium is reached after a few minutes of growth, and the chemical composition of the alloyed Qdots reflects the injected precursor concentration ratio of Te to Se.

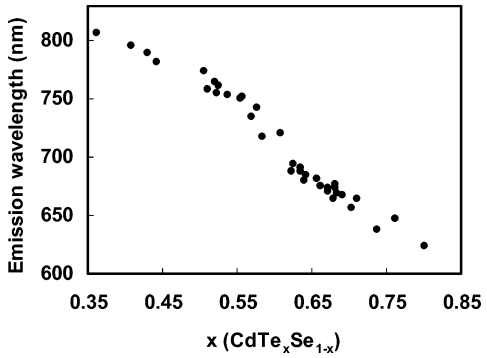

Figure 5. Relationship between Qdot composition and emission wavelength. The emission wavelength of the Qdots is strongly dependent on their Te and Se composition. Elemental analysis was conducted by acid digestion followed by ICP-AES analysis.

the Supporting Information, Figure 1) and have bright and tunable emissions (600−850 nm), quantum yields between 30 and 50%, and 40−50 nm fluorescence fwhm.

Capping the Surface of the Core CdTeSe Qdots with a CdS Shell. For long-term biological studies, the physical and chemical properties and photostability of Qdots are of utmost importance. Previous studies have found that capping binary Qdots (e.g., CdSe) with a shell of wider band gap inorganic material (ZnS) leads to significant enhancement in the fluorescence quantum yields and also minimizes the breakdown of the Qdot by oxidation.[30−32] Furthermore, capping of binary Qdots with inorganic shells of ZnS or CdS has been implicated in higher detection sensitivities and reduced cytotoxicity in biological imaging applications.[35] Although the successful capping of binary Qdots with inorganic shells of higher band gap energies has been achieved using ZnS and CdS,[30,31,33] the ability to coat the $CdTe_xSe_{1-x}$ Qdots may be more difficult because of lattice mismatches from the large differences in bond lengths. We attempted to cap the $CdTe_xSe_{1-x}$ Qdots at different temperatures, with various capping precursor concentrations and injection rates; we had difficulties in reproducibly forming a ZnS shell on the alloyed Qdots (for every 10 attempts, we would produce 1 successful set of Qdots with shell formation). We suspected inconsistent shell formation was a result of interfacial strain from the large lattice mismatches between the $CdTe_xSe_{1-x}$ core and ZnS shell (lattice parameters for $CdTe_{0.5}Se_{0.5}$ are $a = 4.44$ Å, $c = 7.259$ Å, and for ZnS are $a = 3.81$ Å, $c = 6.26$ Å). For $CdTe_xSe_{1-x}$ wurtzite structures, the lattice mismatch between ZnS and $CdTe_xSe_{1-x}$ becomes significant as x starts to increase. We hypothesized that CdS should form capping shells more easily than ZnS because of smaller lattice mismatches (CdS has lattice parameters of $a = 4.16$ Å, $c = 6.756$ Å). Indeed, we found that CdS consistently formed on the surface of the alloyed Qdots and conferred favorable optical properties. Initially, we used a photobleaching test to verify the capping of a CdS shell onto the surface of the alloyed Qdots. Previous studies showed that CdS or ZnS-capped CdSe Qdots were more stable

(30) Peng, X.; Schlamp, M. C.; Kadavanich, A. V.; Alivisatos, A. P. *J. Am. Chem. Soc.* **1997**, *119*, 7019−7029.
(31) Dabbousi, B. O.; Rodriguez-Viejo, J.; Mikulec, F. V.; Heine, J. R.; Mattoussi, H.; Ober, R.; Jensen, K. F.; Bawendi, M. G. *J. Phys. Chem. B* **1997**, *101*, 9463−9475.
(32) Hines, M. A.; Guyot-Sionnest, P. *J. Phys. Chem. B* **1996**, *100*, 468−471.
(33) Schreder, B.; Schmidt, T.; Ptatschek, V.; Winkler, U.; Materny, A.; Umbach, E.; Lerch, M.; Mu1ller, G.; Kiefer, W.; Spanhel, L. *J. Phys. Chem. B* **2000**, *104*, 1677−1685.
(34) Cordero, S. R.; Carson, P. J.; Estabrook, R. A.; Strouse, G. F.; Buratto, S. K. *J. Phys. Chem. B* **2000**, *104*, 12137.
(35) van Sark, W.; Frederix, P.; Van den Heuvel, D. J.; Gerritsen, H. C.; Bol, A. A.; van Lingen, J. N. J.; Donega, C. D.; Meijerink, A. *J. Phys. Chem. B* **2001**, *105*, 8281−8284.

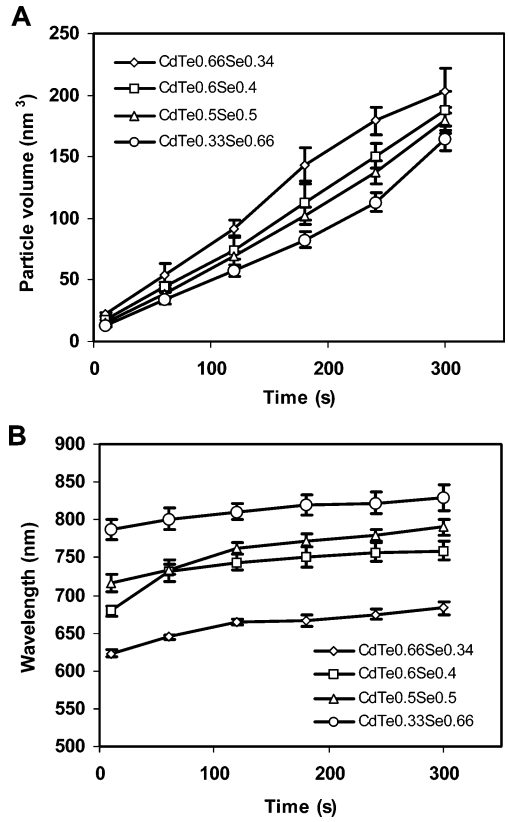

Figure 6. Relationship between Qdot size and emission wavelength vs growth time for different injected precursor concentrations. (A) Increase in Qdots size with growth time. Qdots samples were isolated at different time points and analyzed by TEM. (B) Evolution of Qdots emission wavelength with growth time; the increase in Qdots size can be correlated with the increase in emission wavelength.

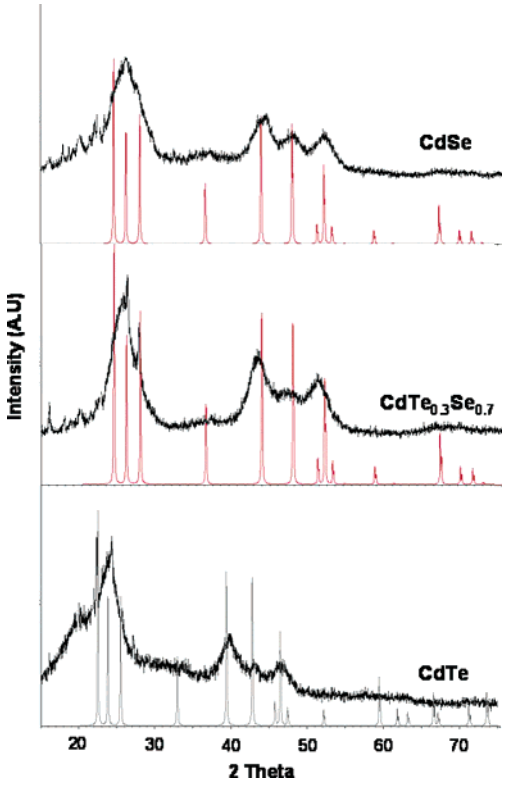

Figure 7. Powdered XRD patterns of pure CdSe, CdTe, and alloyed $CdTe_{0.3}Se_{0.7}$ Qdots. The PXRD data reveal that the alloyed Qdots have a wurtzite structure, as indicated by a large peak at a lower angle followed by three smaller peaks at higher angles. The PXRD spectra of the alloyed Qdots shift toward the spectra of pure CdTe Qdots when there is more than 50% Te in the alloyed Qdots, and vice versa.

against photobleaching than uncapped CdSe Qdots.[29] These Qdots were found to be significantly more stable against photobleaching than uncapped $CdTe_xSe_{1-x}$ Qdots (see Figure 8A). Further, we confirmed the formation of a CdS layer by energy dispersive X-ray spectroscopy (EDX). Figure 8 compares the samples of both capped and uncapped $CdTe_{0.5}$-$Se_{0.5}$ Qdots. The EDX spectra clearly showed the presence of the sulfur peak at $K = 2.3$ eV in the capped sample, indicating the presence of sulfur content in the alloyed Qdots, whereas we did not observe this peak for the uncapped alloyed Qdots. These measurements are also not from CdS Qdots, because we did not observe a fluorescence peak in the UV-to-blue region of the fluorescence spectrum (which is the emission range for this type of Qdots). The thickness of the CdS capping was assessed using ICP-AES. Typically, we observed a capping of one monolayer; for example, using ICP-AES, we measured the S:(Te + Se) ratio to be 0.15−0.20 for 6 nm $CdTe_{0.5}Se_{0.5}$/CdS Qdots. This corresponds to a capping layer thickness of ∼3 Å or about a monolayer of CdS capping; a greater capping layer thickness often results in a significant loss of fluorescence of the Qdots.

Unlike the binary Qdots, we observed that the addition of the CdS capping layer on the Qdot surface resulted in an immediate reduction in the fluorescence yield of the alloyed Qdots. However, such a decrease in fluorescence was not very significant (∼10−20%), and the fluorescence yield of the Qdots often tended to recover after exposure of the alloyed Qdots to room light and temperature. On the basis of previous reports and experimental data, we speculated three possible mechanisms for the increase in fluorescence yield after the initial drop. The three possibilities were photo-oxidation, photobrightening, and photoannealing. With Qdot photo-oxidation, studies showed that Qdots can have an increase in fluorescence, followed by a decrease in the fluorescence signal and a shift in the fluorescence emission to the blue.[34,35] For photobrightening effects, the increase in fluorescence is only temporary, as the enhancement is stopped once the optical excitation source is removed.[36] The photoannealing effect is observed only in core−shell systems, in which the increase in fluorescence is due to the structural rearrangement at the core−shell interface.[37] On the basis of these previous studies, we measured the fluorescence intensity and peak of the alloyed Qdots at various UV exposure times ($\lambda = 365$ nm) and found that the increase in fluorescence intensity was permanent and no spectral blue-shift was observed (see the Supporting Information, Figure 2). These results suggested that photo-oxidation and photobrightening were probably not the cause of this enhancement. Photoannealing, however, was most likely the main cause of this phenomenon, because the enhancement was permanent with no spectral shift. A more detailed photophysical study will be required to provide a better insight into the

(36) Yu, J. Q.; Liu, H. M.; Wang, Y. Y.; Fernandez, F. E.; Jia, W. Y.; Sun, L. D.; Jin, C. M.; Li, D.; Liu, J. Y.; Huang, S. H. *Opt. Lett.* **1997**, *22*, 913−915.
(37) Manna, L.; Scher, E. C.; Li, L.; Alivisatos, A. P. *J. Am. Chem. Soc.* **2002**, *124*, 7136.

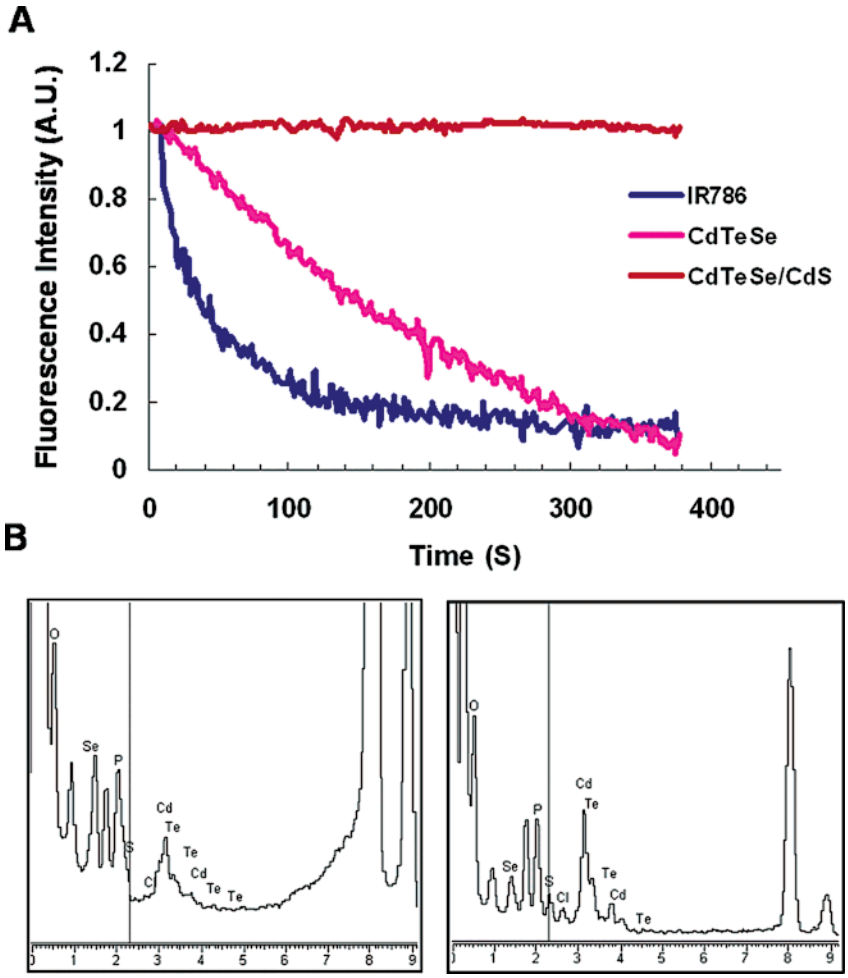

Figure 8. Characterization of $CdTe_xSe_{1-x}$/CdS core/shell Qdots. (A) Photobleaching study of CdS-capped Qdots vs non-capped Qdots and IR786 dye. After ca. 300 s of continuous optical excitation, both the IR786 dye and non-capped Qdots lost nearly 100% of their fluorescence, whereas the fluorescence intensity of the CdS-capped alloyed Qdots was maintained. (B) EDX of $CdTe_xSe_{1-x}$ (left) and $CdTe_xSe_{1-x}$/CdS Qdots (Right). The evidence of sulfide capping layer is indicated by the presence of the sulfur peak at $K = 2.3$ eV. Samples were washed excessively to minimize possible contaminations.

mechanism behind the photoenhancement effects of alloyed Qdots.

Surface Modification of Alloyed Qdots to Interface with Biological Systems. We modified the surface chemistry of these alloyed Qdots using the technique of Jiang et al. to permit their interface with biological systems.[29] Briefly, we exchanged the TOPO molecules on the Qdot surface with mecarptoundecanoic acid, followed by cross-linking the surface mercaptundecanoic acid with the amino acid lysine. We found that, in most batches, the water-soluble alloyed Qdots were monodisperse, highly fluorescent, and stable against flocculation (in pH >7.5). We characterized the surface modification using FT-IR spectroscopy, TEM, optical imaging, and gel electrophoresis (see the Supporting Information, Figures 3 and 4). These alloyed Qdots contained both carboxylic acid and amine functional groups on their surface for attaching biorecognition molecules (e.g., antibodies).

Comparison of Alloyed Qdots to Far-Red- and Near-IR-Emitting Organic Fluorophores. We compared the optical properties of these capped-alloyed Qdots with those of commonly used far-red- to near-IR-emitting organic fluorophores (Cy5.5 and IR-786). In Figure 9A, we show that the fluorescence emission spectra of the near-IR-emitting Qdots are narrower than the Cy5.5 emission spectrum (~40 nm full width at half-maximum for the Qdots in comparison to the 60 nm for the Cy5.5 dye). Also, the fluorescence spectrum of the Qdots is symmetric and narrow and does not contain a front or tail. The relative fluorescence quantum yield of our alloyed near-IR-emitting Qdots was calculated by comparison with IR-786, an organic fluorophore with near-IR emission and a reported quantum yield of 15.9% in methanol (Figure 9B).[8] By synthesizing Qdots with matching fluorescence emission wavelength to IR-786 and using excitation wavelengths at which the absorption of both the Qdots and dye were equal, the relative quantum yield was calculated using the ratio of the integrated fluorescence intensities of the Qdots and the IR-786 (Figure 9B). On the basis of this measurement, the fluorescence quantum yields of the near-IR emitting Qdots are three times the quantum yield of IR-786, or roughly 35−40%. In fact, the Qdots with an emission range of 600−850 nm had typical quantum yields of 30−50%, which is one of the highest reported relative quantum yield for water-soluble Qdots in the 600−850 nm emission range. These Qdots are bright enough to be imaged at the single nanoparticle level (see the Supporting Information, video SV1).

We conducted further comparative studies of the Qdots to organic fluorophores in order to demonstrate the value of using near-IR-emitting Qdots for biological imaging applications. In particular, we compared the signal:noise ratio (SNR)

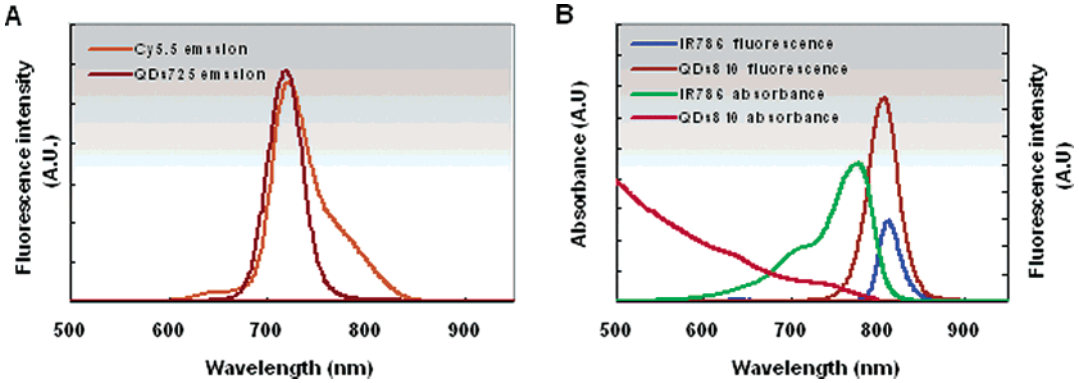

Figure 9. Comparison of the fluorescence emission of near-IR emitting Qdots and organic fluorophores. (A) The fluorescence emission spectrum of 720 nm emission Qdots is narrow (fwhm is ca. 40 nm) and symmetric, whereas the Cy5.5 dye has a broad emission spectrum (fwhm is ca. 60 nm) with a long red tail. (B) Quantum yield comparison of 820 nm emitting Qdots and IR786 dye. The excitation wavelengths for the two dyes are selected so that both fluorophores absorb the same number of photons (abs = 0.10). The integrated areas under the fluorescence peaks indicate the relative quantum yields of the fluorophores; the near-IR-emitting Qdot has nearly three times the area and, hence, three times the quantum yield (>40%) of IR-786 (QY = 15% in methanol).

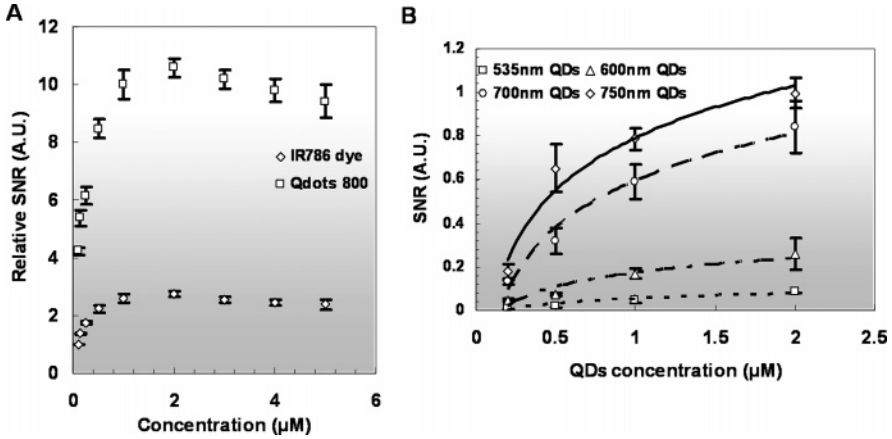

Figure 10. Signal:noise ratio (SNR) comparison of near-IR-emitting organic fluorophores, visible-emitting Qdots, and alloyed Qdots. Mixed with HeLa cell homogenates, (A) 810 nm emitting Qdots showed a significantly higher SNR than IR786 dye at all fluorophore concentrations. In these experiments, the excitation wavelength was adjusted so that the samples were excited at the same absorbance values. (B) We compared the relative SNR of the visible emitting ZnS-capped CdSe Qdots to that of the alloyed Qdots in cell homogenates. The 750 nm Qdots had a much higher SNR than Qdots with shorter emission wavelengths. All Qdots were excited at a wavelength of 450 nm. All solid lines are logarithmic fits of the data points.

of Qdots and organic fluorophores mixed with homogenized cells and tissues, respectively. HeLa cells were mixed with different concentrations of either 800 nm emitting Qdots or IR786 dye. SNR was obtained by calculating the ratio between the measured fluorescence of fluorophores incubated with cells and measured fluorescence of cells without any fluorophores. As expected, the SNR increased as the concentration of the fluorophores increased (see Figure 10A). However, cell homogenates incubated with Qdots exhibited a much higher SNR (4−5× higher) than the cell-dye mixtures at all fluorophore concentrations. This improved SNR can be attributed to the higher quantum yields of the near-IR-emitting Qdots as compared with IR-786. We further compared the near-IR emitting alloyed Qdots to those of the visible-emitting ZnS-capped CdSe Qdots. Figure 10B shows that the SNR can be improved more than 10-fold when comparing 750 nm emitting Qdots to 535 nm emitting Qdots in cell homogenates. The increase in SNR at longer wavelength is mainly due to the low cellular autofluorescence in the near-IR spectrum. In addition, there could a further improvement in the optical sensitivity for imaging tissues, organs, or whole animal because of the reduced optical noise from tissue absorption and scattering in the near-IR emission range. These results further demonstrate the importance of the development of near-IR-emitting Qdots for highly sensitive bioimaging and detection applications.

Conjugation of Biorecognition Molecules to Qdots. To use these alloyed Qdots as a targeted contrast agent for cell, tissue, and animal imaging, they need to be conjugated with specific biorecognition molecules. To the best of our knowledge, there are no reports of conjugation of biorecognition molecules with alloyed Qdots. We used transferrin, an iron-transporting protein, to make Qdot bioconjugates. The water-soluble alloyed Qdots were conjugated to transferrin by using the EDC method, as described in a previous publication.[29] The Qdot conjugates were delivered into cells via the transferrin receptor-mediated endocytosis pathway. Cell labeling was performed with HeLa cells in cultures with the presence of Qdot−transferrin conjugates. Figure 11 showed images of the cells labeled with the near-IR-emitting Qdots. The Qdots accumulated in vesicles within the cells.[38] To validate Qdot labeling specifically through the uptake of transferrin conjugation, we performed control experiments

(38) Jaiswal, J.; Mattoussi, H.; Mauro, J. M.; Simon., S. M. *Nat. Biotechnol.* **2003**, *21*, 47−51.

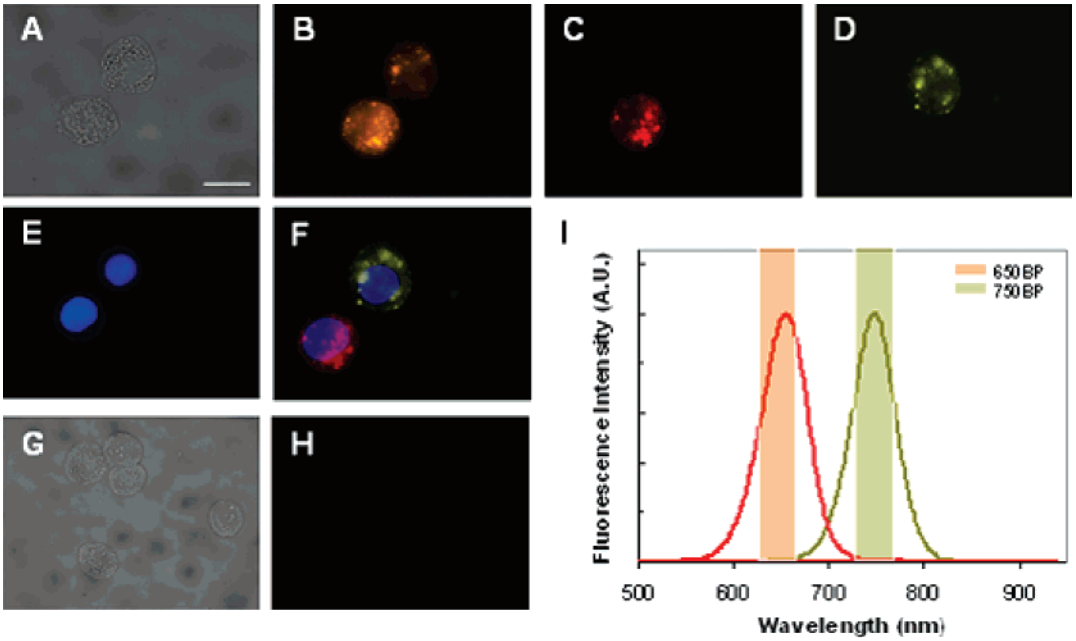

Figure 11. Multiplexed in vitro imaging of HeLa cells stained with near-infrared-emitting Qdots. Two different populations of HeLa cells were incubated with 660 nm emitting (pseudo-colored red) and 750 nm emitting (pseudo-colored green) near-IR-emitting Qdots (A−F) with or (G−H) without conjugation to transferrin. Upon trypsinization and mixing of the two cell populations into a single culture dish, DIC (A,G) and fluorescence (B−F,H) images were taken. Spectral resolution and sorting of HeLa cells labeled with transferrin-conjugated near-infrared-emitting Qdots is demonstrated by taking fluorescence images (B−D) using (B) 650LP, (C) 650/40BP, and (D) 750/40 BP emission filters. (E) Image of HeLa cell nuclei stained with DAPI, taken using a 460/50 BP emission filter. (F) Superimposed image of (C−G) demonstrating that transferrin-conjugated near-IR-emitting Qdots are located in perinuclear regions within the HeLa cells. (G) Control DIC and (H) fluorescence image of two HeLa cell populations incubated with near-IR-emitting Qdots without transferrin conjugation (B−F). (I) Fluorescence spectra of near-IR-emitting Qdots and emission filter selection corresponding to fluorescence images (C,D). LP = long pass and BP = band pass. Scale bar = 10 μm.

with (1) incubation of cells with unconjugated near-infrared-emitting Qdots and (2) incubation of cells with nontargeting protein (e.g., bovine serum albumin). In both of these controls, no Qdot signals were present, whereas cell labeling was positively achieved with the transferrin-conjugated Qdots (Figure 11). Unlike the silica-coated Qdots,[13] there was minimal nonspecific ingestion of these particular Qdots by the cells.

Given successful labeling and imaging of cells with these Qdots, we next tested if multiple far-red- to near-IR-emitting Qdots can be spectrally differentiated. This approach of multiplex labeling of cells, tissues, and organs will provide a capacity to assess multiple-target molecules simultaneously for detection of specific cell populations in biological imaging and medical diagnostics. Using two different emitting Qdots, we labeled HeLa cells in separate cultures. The two cell populations were then mixed and prepared on cytospin slides for examination of Qdots signals by using an epifluorescence microscope. As shown in Figure 11, two sets of cells labeled with different emitting Qdots can be optically distinguished using the appropriate filter system. Furthermore, we showed that three different sets of near-IR-emitting Qdots can be distinguished using the appropriate optical filters (see the Supporting Information, Figure 5). Realistically, with our set of prepared alloyed Qdots, we predict that we can optically resolve at least five near-IR-emitting Qdots (with emission filters of ±30 nm) within the near-IR emission window. This cannot be done using currently commercial near-IR-emitting organic fluorophores (because of their broad fluorescence emission). With the high-quality ZnS-capped CdSe Qdots and these CdS-capped $CdTe_xSe_{1-x}$ Qdots, we can realistically resolve 12 colors within the fluorescence emission range of 480−850 nm, and all of these colors could be excited using a single wavelength.

Conclusions

We systematically studied the growth kinetics of alloyed Qdots and discovered that the synthetic conditions have to be optimized in order to prepare high-quality far-red- to near-IR-emitting Qdots. We developed and characterized CdS-capped alloyed $CdTe_xSe_{1-x}$ Qdots with fluorescence emission wavelengths ranging from 600 to 850 nm (visible to near-infrared light), narrow spectral linewidths (<50 nm), high quantum yields (>30%), and stability against photobleaching. We demonstrate the formation of inorganic CdS shells on the near-IR-emitting core $CdTe_xSe_{1-x}$ Qdots, which is important in producing Qdots with high fluorescence quantum yields, long-term photostability, and low cytotoxicity. We further demonstrate the conjugation of near-IR-emitting Qdots to biorecognition molecules, and demonstrate the multiplexed labeling and detection of different cell populations using near-IR-emitting Qdots with unique fluorescence emission wavelengths. On the basis of the narrow spectral linewidths of the CdS-capped alloyed $CdTe_xSe_{1-x}$ Qdots, we estimate that it is possible to spectrally resolve at least five near-IR-emitting Qdots (with 30 nm bandwidth filters) within the near-IR window. Thus, using both high-quality ZnS-capped CdSe Qdots and these CdS-capped $CdTe_xSe_{1-x}$ Qdots, we can realistically perform multiplexed imaging using 12 fluorescence emission colors within the wavelength range of 480 to 850 nm and only a single excitation wavelength. These advancements pave the way for novel biological

applications of near-IR emitting Qdots, including cell and histological staining, targeted in vivo molecular imaging, high-throughput cell sorting, and molecular diagnostics.

Acknowledgment. We thank Dr. Sergey Petrov for the help with PXRD and Dr. Neil Coomb for helping with TEM. We also thank Jonathan Lai, Hans Fischer, Jesse Klostranec, Dr. Travis Jennings, and Dr. Christopher Yip for helpful discussions. W.C. and C.W. acknowledge CIHR (NET in Regenerative Medicine and Nanomedicine and Novel Tools Grant). W.C. also acknowledges NSERC, CFI, and OIT; and W.J. and A.S. thank OGS and NSERC, respectively, for student funding.

Supporting Information Available: Characterizations of Qdots, including FTIR spectra of TOPO, MUA, and lysine-cross-linked, MUA-coated Qdots, gel electrophoresis of water-soluble, near-IR-emitting Qdots, movie of monodisperse water soluble NIR Qdots, and multiplexed imaging of Qdots encoded beads. This material is available free of charge via the Internet at http://pubs.acs.org.

CM061311X